Journal of Applied Polymer Science

Characterization and strain-energy-function-based modeling of the thermomechanical response of shape-memory polymers

Sesha S. Pulla, Mohammad Souri, Haluk E. Karaca, Y. Charles Lu
Department of Mechanical Engineering, University of Kentucky, Lexington Kentucky 40506
Correspondence to: Y. C. Lu (E-mail: ycharles.lu@uky.edu)

ABSTRACT: Shape-memory polymers (SMPs) are an emerging class of active polymers that can be used on a wide range of reconfigurable structures and actuation devices. In this study, an epoxy-based SMP was synthesized, and its thermomechanical behaviors were comprehensively characterized. The stress–strain behavior of the SMP was determined to be nonlinear, finite deformation in all regions. Strain-energy-based models were used to capture the complicated stress–strain behavior and shape-recovery response of the SMP. Among various strain energy functions, the stretch-based Ogden model provided the best fit to the experimental observations. Compared to the sophisticated models developed for SMPs, the strain-energy-based model was found to be reliable and much easier to use for practical SMP designs. © 2015 Wiley Periodicals, Inc. J. Appl. Polym. Sci. **2015**, *132*, 41861.

KEYWORDS: properties and characterization; stimuli-sensitive polymers; theory and modeling

Received 4 September 2014; accepted 9 December 2014
DOI: 10.1002/app.41861

INTRODUCTION

Shape-memory polymers (SMPs) are a group of active materials that that have been considered for the development of reconfigurable structures and actuation devices.[1–5] The shape-memory effect in polymers stems from their unique molecular structures. A typical polymer is a mixture of many long, entangled molecular chains that are connected via characteristic netpoints (chemical crosslinking or physical crosslinking).[6] At temperatures higher than the glass-transition temperature (T_g), those polymer chains are relaxed and flexible. As a result, the polymer becomes soft and is characterized as being in the rubbery state. When an external stress is applied, the polymer chains can be readily deformed, and the netpoints may also be displaced. As the temperature is reduced below the transition temperature while the polymer maintains its predeformed shape, some secondary crosslinks can be formed among those deformed polymer chains. These help fix the polymer in the temporary shape once the external stress is removed. When the polymer is reheated above its transition temperature, those secondary crosslinks are released, and the original shape is recovered.

The design of SMP-based structures and devices requires thorough characterization and constitutive modeling of the thermomechanical behavior of the materials. Many phenomenological and micromechanics-based constitutive models are available for SMPs, although most of them have focused on small deformations (<10% nominal strain for compression or tension). Tobushi and coworkers[7,8] have developed a spring–dashpot system to model the behavior of SMPs for small deformations. The model was later improved by the incorporation of thermal expansion and some nonlinear elastic terms.[9,10] Srinivasa and Gosh[11] subsequently developed a rheological-based model by also using the spring–dashpot analogy. A phenomenological based model was developed by Liu *et al.*,[12] in which the SMP is treated as a material consisting of two phases: the frozen phase and the active phase. The material becomes frozen at low temperatures and then active upon heating; this allows the stored deformation to return to the original shape. Following the framework of Liu *et al.*, Chen and Lagoudas[13,14] developed a three-dimensional constitutive model for SMPs.

The existing models often have a large number of material parameters, for instance, more than 17 in the model of Qi *et al.*,[15] 18 in the model of Hong *et al.*,[10] and up to 45 in the model of Srivastava and Gosh.[11] To accurately acquire such a large number of material parameters would require specific experiments and complex calibration processes. Therefore, although some models are very comprehensive and capable of capturing the complex behaviors of SMPs, they are difficult to use in practice, and none of these models have been implemented in commercial analysis codes. In this study, an epoxy-based SMP was synthesized, and its thermomechanical behavior was characterized by compression. Strain energy functions, commonly used for the modeling of the large deformation of elastomeric materials, were used to model the stress–strain and shape-recovery responses of the SMP.

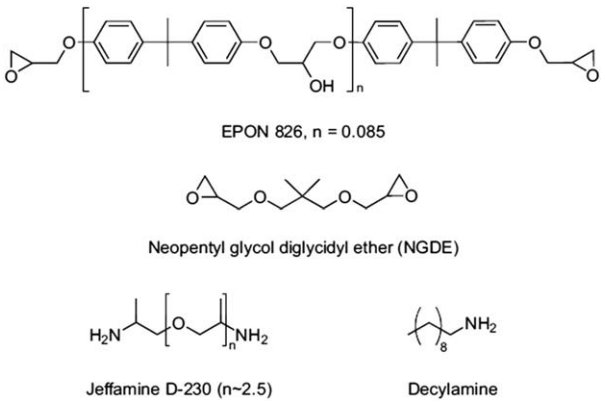

Figure 1. Chemical structures of the components used in the epoxy-based SMP. Reprinted with permission from ref. 25. Copyright 2009 Elsevier.

EXPERIMENTAL

Materials and Sample Preparation

An epoxy-based SMP was used in this study. The polymer was composed of the following substances: (1) diglycidyl ether of bisphenol, an epoxy monomer (EPON 826, available from Hexion); (2) a curing agent, poly(propylene glycol)bis(2-aminopropyl) ether (Jeffamine D230, available from Huntsman); and (3) neopentyl glycol diglycidyl ether (NGDE), manufactured by TCI America. The chemical structures of these reactants are shown in Figure 1. To synthesize the SMP, the EPON 826 was first placed in the furnace and heated to 80°C for 10 min to reduce its viscosity. The treated EPON 826 was then removed from the furnace and mixed with the other two ingredients. The solution was stirred for 15–30 s to ensure the proper mixing and then placed *in vacuo* at 20-in. Hg for about 2 min to remove the bubbles that developed during the mixing. The liquid SMP was subsequently poured into a cylindrical Teflon mold and placed in a furnace for curing at 100°C for 1.5 h. After cooling, the samples were removed from the mold and polished to ensure smooth surfaces.

Transition Temperature

The transition temperature of the SMP was characterized with differential scanning calorimetry (DSC; PerkinElmer Pyris1 differential scanning calorimeter). We operated he DSC instrument by recording the amount of heat required to increase the temperature of the material versus a change in the temperature. Small-sized samples, weighing about 5 mg, were used for the experiment. The sample was heated from 25 to 70°C at a rate of 2°C/min.

Stress–Strain Tests

The stress–strain behavior of the SMP was obtained through an isothermal, uniaxial compressive test conducted on a BOSE ElectroForce load frame system. The specimens were small cylinders with a nominal height of 11 mm and a nominal diameter of 6.25 mm. In each test, the specimen was first placed on the bottom testing platen and then heated up to a desired temperature, from 30 to 60°C. A minimum of 10 min was given to allow the specimen to reach thermal equilibrium. The uniaxial compressive tests were conducted under the force–control mode through the application a compressive force of up to 2000 N at a rate of 2 N/s.

Shape-Recovery Tests

The shape-recovery tests were conducted with cylindrical shaped specimens, the same size specimens as used in compressive tests. The tests were carried out in a servohydraulic MTS LandMark testing system equipped with a custom built cooling–heating system. An Omega CN8200 temperature controller was used to control the temperature of the thermal chamber. The actual temperature of the sample was measured by a K-type thermocouple attached to the sample and the compression grips. The shape-recovery tests followed the standard thermomechanical cycle. First, the specimen was placed on the bottom testing platen and then heated to the rubbery state (60°C). After the temperature reached equilibrium, the specimen was compressed to a desired strain ($\varepsilon_0 \approx 18\%$). With the strain held constant, the specimen was cooled to the glassy state (12°C). Once the cooling was completed, the load was removed, and the SMP remained fixed. Finally, the specimen was reheated to the original temperature (60°C) for recovery (unconstrained recovery). The rate of heating or cooling used in the experiment was kept constant, that is, at 2°C/min.

STRAIN-ENERGY-FUNCTION-BASED MODELING

For isotropic, incompressible materials that are subjected to uniaxial tension or compression, Rivlin[16] showed that

$$\frac{\sigma}{(\lambda-\lambda^{-2})} = 2\left[\frac{\partial W}{\partial I_1} + \frac{1}{\lambda}\frac{\partial W}{\partial I_2}\right] \tag{1}$$

where σ is the engineering stress, λ is the stretch ratio, and W represents the strain energy function:

$$W = f(I_1, I_2, I_3)$$

where I_1, I_2, and I_3 are the three invariants given in terms of the principal stretch ratios λ_1, λ_2, and λ_3, respectively.

Mooney–Rivlin Strain Energy Function

There exist various strain energy functions for modeling materials that undergo finite deformation. By assuming impressibility ($I_3 = 1$), Rivlin[16] proposed that the strain energy function be expressed in the power series:

$$W = \sum_{i+j=1}^{\infty} C_{ij}(I_1-3)^i(I_2-3)^j \tag{2}$$

Taking only the first two terms ($i = j = 1$) in eq. (2) results in the Mooney–Rivlin strain energy function:

$$W = \sum_{i+j=1}^{\infty} C_{ij}(I_1-3)^i(I_2-3)^j = C_{10}(I_1-3)+C_{01}(I_2-3) \tag{3}$$

Substituting eq. (3) into eq. (1) yields

$$\frac{\sigma}{(\lambda-\lambda^{-2})} = 2C_{10} + \frac{1}{\lambda}2C_{01} \tag{4}$$

Through the plotting of $\sigma/(\lambda - \lambda^{-2})$ versus $1/\lambda$, the constants C_{10} and C_{01} can be estimated.

Yeoh Strain Energy Function

On the basis of the experimental observations, Yeoh[17] has noticed that $\partial W/\partial I_1$ is much greater than $\partial W/\partial I_2$. Therefore, Yeoh proposed that the second term be neglected in generalized

strain energy function, as shown in eq. (3), which resulted in Yeoh's model:

$$W = \sum_{i=1}^{\infty} C_i (I_1 - 3)^i = C_{10}(I_1 - 3) + C_{20}(I_1 - 3) + C_{30}(I_1 - 3) \quad (5)$$

The substitution of eq. (5) into eq. (1) yields

$$\frac{\sigma}{(\lambda - \lambda^{-2})} = 2C_{10} + 4C_{20}(I_1 - 3) + 6C_{30}(I_1 - 3)^2 \quad (6)$$

Through the plotting of $\sigma/(\lambda - \lambda^{-2})$ versus $(I_1 - 3)$, the constants C_{10}, C_{20}, and C_{30} can be estimated.

Ogden Strain Energy Function

In contrast with the invariant-based strain energy function, Ogden proposed to derive W in terms of stretch ratios; this results in a stretch-based strain energy function:[18,19]

$$W = \sum_{i=1}^{n} \frac{\mu_n}{\alpha_n} (\lambda_1^{\alpha_n} + \lambda_2^{\alpha_n} + \lambda_3^{\alpha_n} - 3) \quad (7)$$

where μ_n and α_n are material constants. In simple tension or compression, we have $\lambda_1 = \lambda$ and $\lambda_2 = \lambda_3 = \lambda^{-1/2}$. With the first two terms, eq. (8) reduces to

$$W = \frac{\mu_1}{\alpha_1} (\lambda^{\alpha_1} + 2\lambda^{-\frac{\alpha_1}{2}} - 3) + \frac{\mu_2}{\alpha_2} (\lambda^{\alpha_2} + 2\lambda^{-\frac{\alpha_2}{2}} - 3) \quad (8)$$

The substitution of eq. (9) into eq. (1) yields

$$\sigma = \mu_1 (\lambda^{\alpha_1 - 1} - \lambda^{-\frac{\alpha_1}{2} - 1}) + \mu_2 (\lambda^{\alpha_2 - 1} - \lambda^{-\frac{\alpha_2}{2} - 1}) \quad (9)$$

By curve fitting, the constants μ_1,α_1, μ_2, and α_2 can be estimated.

Neo–Hooke Strain Energy Function

On the basis of the physics of polymer chain networks, a few micromechanical-based strain energy functions have been developed. The simplest one among those types of functions is the Neo–Hooke model:[20]

$$W = C_{10}(I_1 - 3) \quad (10)$$

where C_{10} is equal to $\frac{1}{2}nkT$, n is the chain density per unit of volume, k is the Boltzmann constant, and T is the absolute temperature. The only material parameter, C_{10}, denotes the initial shear modulus, $\mu = 2C_{10}$.

Substituting eq. (11) into eq. (1) yields

$$\frac{\sigma}{(\lambda - \lambda^{-2})} = 2C_{10} \quad (11)$$

Through the plotting of σ versus $(\lambda - \lambda^{-2})$, the constant C_{10} can be estimated.

Arruda–Boyce Strain Energy Function

Arruda and Boyce recently developed a new micromechanics-based strain energy function:[21]

$$W = \mu \sum_{i=1}^{5} \frac{C_i}{N^{i-1}} (I_1^i - 3^i), \quad [C_1, C_2, C_3, C_4, C_5] = \left[\frac{1}{2}, \frac{1}{20}, \frac{11}{1050}, \frac{19}{7000}, \frac{519}{673750}\right] \quad (12)$$

where N is the number of Kuhn segments per polymer chain.

Through the solution of eq. (13), the stress–stretch relation in simple tension or compression can be obtained:

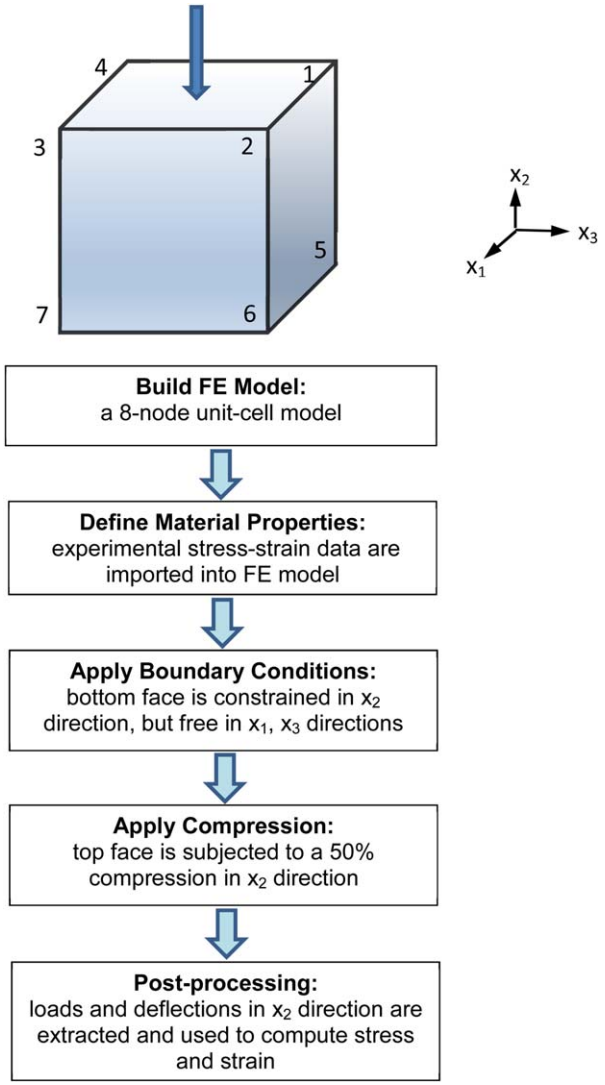

Figure 2. Unit-cell FE model and flowchart used for computing the stress and strain. [Color figure can be viewed in the online issue, which is available at wileyonlinelibrary.com.]

$$\frac{\sigma}{(\lambda - \lambda^{-2})} = \sum_{i=1}^{5} \frac{2\mu i C_i}{N^{i-1}} (I_1^{i-1}) \quad (13)$$

By curve fitting, the constants μ and N can be estimated.

In this study, the coefficients of various strain energy functions were determined with the curve-fitting utility in a commercial finite element (FE) program, ABAQUS.[22] A unit-cell element was built in a Cartesian coordinate system with the axes x_1, x_2, and x_3 (Figure 2). To evaluate the hyperelastic behavior of the SMP, the continuous, reduced-integration, hybrid element (C3D8RH) was used. To conduct compressive testing, a displacement was assigned to a node at the top of the specimen to allow it to deform in the longitudinal axis (x_2 direction). The specimen was free to extend or contract in the x_1 and x_3 directions. The experimental stress–strain data, as shown in Table A.I in the appendix, were entered into the program to compute the coefficients of the strain energy functions.

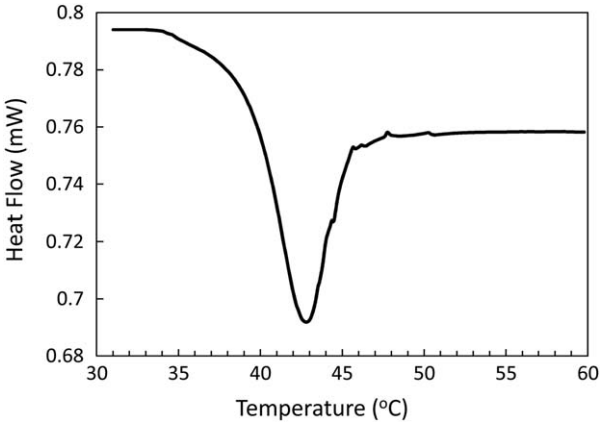

Figure 3. DSC results showing T_g of the SMP.

RESULTS AND DISCUSSION

Transition Temperature

Figure 3 depicts the heat flow versus temperature response of this SMP as measured by DSC. T_g of the SMP was determined as the temperature corresponding to the maximum heat flow: $T_g \approx 43°C$. The transition region started at about 39°C and ended at about 46°C. The SMP could be classified as in the glassy state below 39°C and in the rubbery state above 46°C.

Mechanical Behavior

The mechanical responses of this SMP were examined in compression mode at temperatures spanning all three regions of the polymer: glassy region (30 and 35°C), glassy-to-rubbery transition region (45°C), and rubbery region (50 and 55°C). Figure 4 shows the isothermal compressive stress–strain curves of the SMP at various temperatures. The complete stress–strain data are summarized in Table A.I in the appendix. The material displayed typical hyperelastic behavior in the rubbery regions above T_g. At temperatures below T_g, the material showed inelastic behavior. With increasing strain, the material started to undergo stress softening. As the temperature changed from the glassy state to the rubbery state, the amounts of stress required to achieve the same level of strain decreased dramatically. For example, the stress required to configure the SMP at 30% strain in the glassy state was 32 MPa, whereas the stress to configure the SMP at the same strain in the rubbery state was only 4.5 MPa. This corresponded to a drop of 86%.

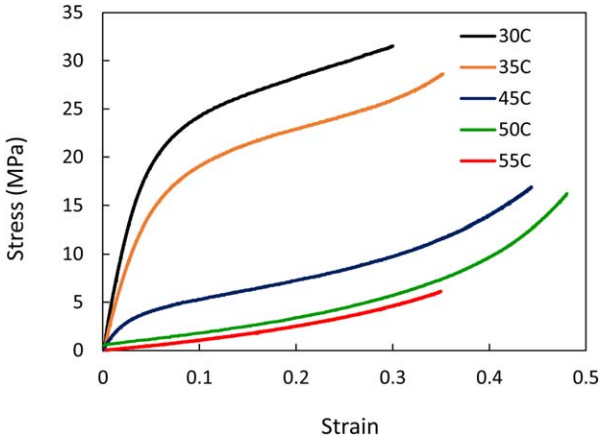

Figure 4. Compressive stress–strain responses of the SMP at various temperatures (30–55°C). [Color figure can be viewed in the online issue, which is available at wileyonlinelibrary.com.]

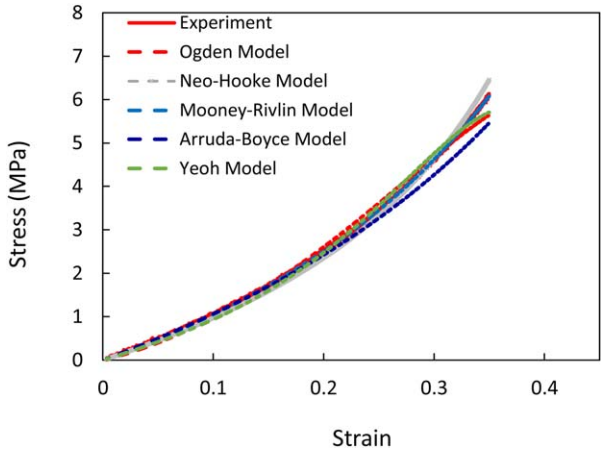

Figure 5. Compressive stress–strain responses of the SMP at 55°C. [Color figure can be viewed in the online issue, which is available at wileyonlinelibrary.com.]

Predictions with Strain Energy Functions

The stress–strain responses of the SMP have been modeled with commonly used strain energy functions (Mooney–Rivlin, Yeoh, Neo–Hooke, Arruda–Boyce, and Ogden). Figures 5–9 show the predicted results at various temperatures.

Figures 5 and 6 show the stress–strain responses of the SMP above the T_g (50 and 55°C) predicted from various strain energy functions. In the rubbery state, the SMP behaved like a typical unfilled rubber. The stresses increased slowly with increasing strain, without any sudden upturns or downturns. Most strain energy functions could successfully predict the responses of the SMP at this state.

As the material moved to the transitional state (45°C; Figure 7) and the glassy state (35 and 30°C; Figures 8 and 9), the stress–strain curves displayed some sudden changes, with noticeable stress softening after the yield points. In those cases, some strain

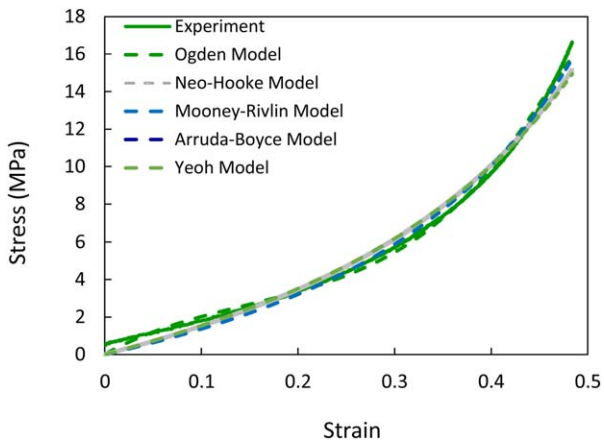

Figure 6. Compressive stress–strain responses of the SMP at 50°C. [Color figure can be viewed in the online issue, which is available at wileyonlinelibrary.com.]

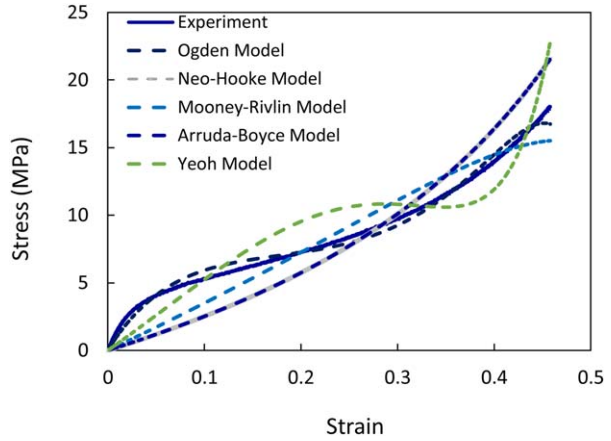

Figure 7. Compressive stress–strain responses of the SMP at 45°C. [Color figure can be viewed in the online issue, which is available at wileyonlinelibrary.com.]

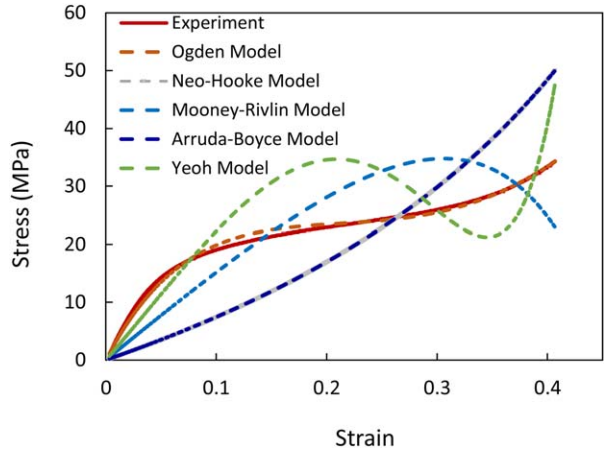

Figure 8. Compressive stress–strain responses of the SMP at 35°C. [Color figure can be viewed in the online issue, which is available at wileyonlinelibrary.com.]

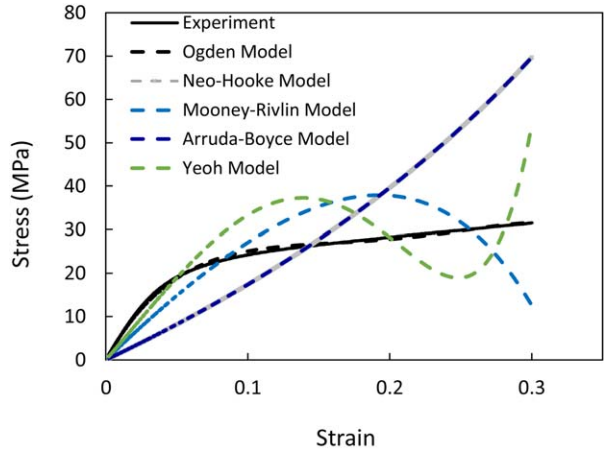

Figure 9. Compressive stress–strain responses of the SMP at 30°C. [Color figure can be viewed in the online issue, which is available at wileyonlinelibrary.com.]

Table I. Comparisons of the Coefficients of the Neo–Hooke and Arruda–Boyce Models

Temperature	Neo–Hooke	Arruda–Boyce	
	C_{10}	μ	N
30°C	25.979	51.958	1159.214
35°C	11.121	22.243	1577.362
45°C	3.763	7.526	1836.209
50°C	2.307	4.548	3.114
55°C	1.590	2.859	1.037

Table II. Summary of the Ogden Coefficients

Temperature	μ_1	α_1	μ_2	α_2
30°C	380.920	18.333	−182.824	−9.277
35°C	241.345	13.313	−117.241	−6.701
45°C	73.8194	14.690	−35.211	−7.425
50°C	16.5839	11.603	−6.782	−6.084
55°C	2.25313	2.064	−0.820	−2.152

energy functions failed to properly capture the responses. The micromechanical-based models, Neo–Hooke and Arruda–Boyce, were derived from molecular chain statistics. The stress–strain responses were mostly predicted by μ of the molecular chain stretching, $2C_{10}$ in the Neo–Hooke model, and μ in the Arruda–Boyce model. As presented in Table I, the μ values predicted from these two models were exactly the same. Because only uniaxial data was used in this study, the second term (N) in the Arruda–Boyce model did not seem to have played any significant role. Therefore, the stress–strain curves predicted from the Arruda–Boyce model overlapped with those from the Neo–Hooke model. Overall, the predictions from the micromechanics-based models deviated from the experimental data because of some significant turns that were present.

Some phenomenological-based models, such as the Mooney–Rivlin and Yeoh models, could capture the initial responses of the material, but they became unstable at large strains. In all

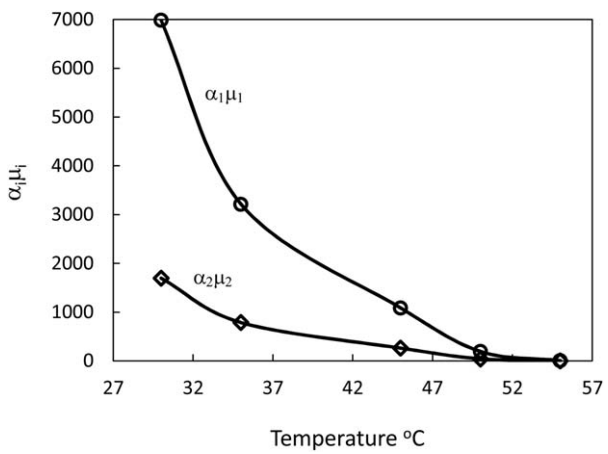

Figure 10. Variations of $\alpha_i\mu_i$ in the Ogden model.

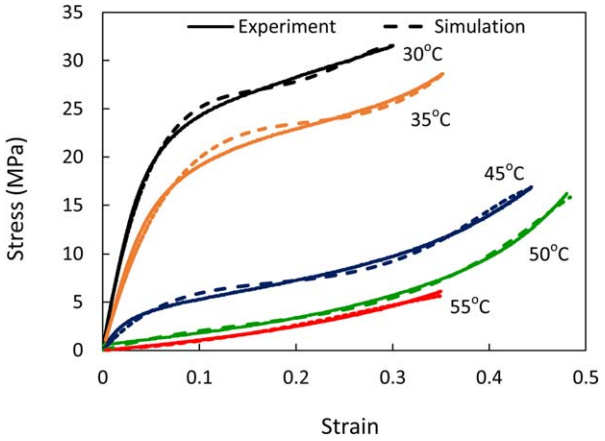

Figure 11. Comparisons of the stress–strain responses of the SMP between the experimental data and the Ogden model. [Color figure can be viewed in the online issue, which is available at wileyonlinelibrary.com.]

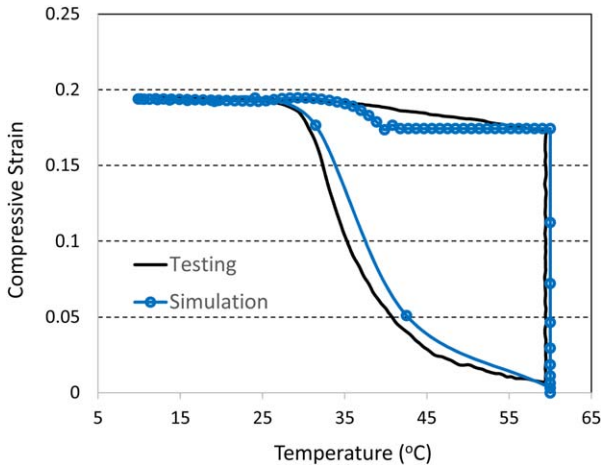

Figure 12. Strain–temperature profiles showing the shape recovery of the SMP. [Color figure can be viewed in the online issue, which is available at wileyonlinelibrary.com.]

cases, the Ogden models seemed to have provided excellent fits to the experimental data. The coefficients of the Ogden models for this SMP are summarized in Table II. In the Ogden model, the free energy density is formulated as a finite sum of scaled powers of the principal stretches, λ_i [eq. (10)]. There are 2_i material constants in the model, the shear modulus, μ_i, and the dimensionless exponent, α_i, and the sum of these two constants is the classical shear modulus:[19]

$$\sum_{i=1}^{n} \mu_i \alpha_i = 2\mu \tag{14}$$

For the model to be stable, $\mu_i \alpha_i > 0$ has to be satisfied. Examining the values of $\mu_i \alpha_i$ shown in Figure 10, we observed that the conditions for stability were met in all cases. Comparisons of the stress–strain curves between the Ogden models and experimental measurements for all of the temperatures are depicted in Figure 11.

The Ogden model was tested further with two additional SMP material systems available in the literature: an epoxy-based SMP[23] and an aramid-based SMP.[24] Detailed information about

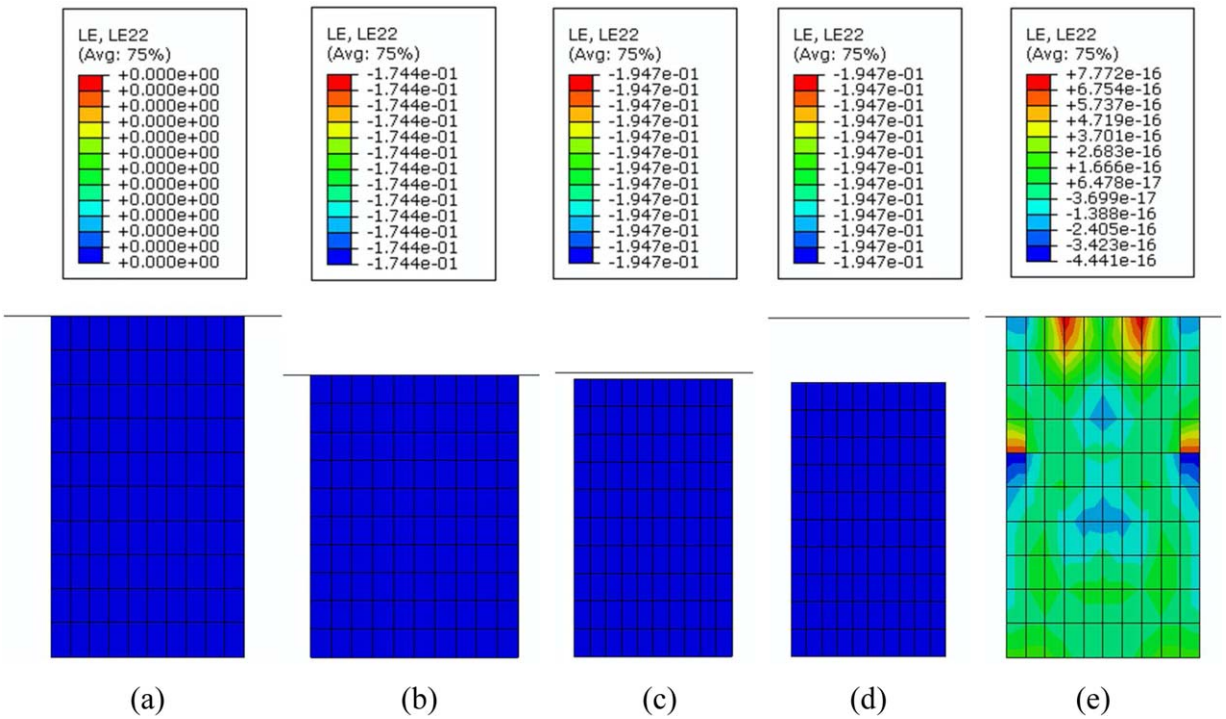

Figure 13. Contours of the compressive strain (LE22 - logarithmic strain in vertical direction) showing the process of shape recovery of the SMP: (a) original shape (heated to 60°C), (b) step 1 (compressed to a strain of 17.5%), (c) step 2 (temperature lowered to 12°C; the strain increased to 19.5% because of thermal contraction), (d) step 3 (compression removed), and (e) step 4 (heated to 60°C again; the strain recovered to ~0%). [Color figure can be viewed in the online issue, which is available at wileyonlinelibrary.com.]

the materials and the predictions are given in the appendix. Overall, the Ogden model provided good predictions of the stress–strain responses of the materials.

Characterization and Modeling of the Shape Recoveries

The shape-recovery ability is important to SMPs because it is the indication of a material's ability to return to its original shape upon programming. The unconstrained shape-recovery tests were conducted according to the standard thermomechanical cycle. Figure 12 shows a breakdown of the complete shape-memory cycle. The material was first heated to a temperature above its glass transition, 60°C. After the temperature had reached equilibrium, the sample was deformed to a compressive strain of approximately 17.5% (step 1). The deformed material was then cooled a temperature below its glass transition, 12°C (step 2). After cooling, the constraint was released, and a permanent shape was fixed on the sample (step 3). This step also showed the material's *shape fixity*, which was its ability to hold a shape after it was deformed. The level of fixing strain was approximately 19.5% at this point; this was slightly increased from the original (17.5%) because of the thermal contraction of the polymer as the temperature dropped from 60 to 12°C. Finally, the material was reheated to the starting temperature of the thermomechanical cycle, 60°C, to recover its shape freely (step 4). The SMP's recovery characteristics could be illustrated by the production of a shape-memory plot of the strain versus temperature. From this plot, the linear shape-recovery ratio (R) could be estimated:

$$R = (1-\frac{\varepsilon_f}{\varepsilon_i})\times 100 \quad (15)$$

where ε_i and ε_f are the initial and final strains of the cylindrical specimens, respectively. We observed that after the final step, the SMP returned completely to its original position, and the estimated linear R was 100%.

The shape-recovery process under unconstrained conditions could be simulated through the FE method with the Ogden strain energy function (Table II). The commercial nonlinear FE code ABAQUS was used.[22] The actual cylinder-shaped specimen was modeled with axisymmetric, hybrid elements, and the compression platen was modeled with a rigid surface. The contact between the specimen and indenter was treated as frictionless. The base of the specimen was constrained in the vertical direction, whereas the nodes along the center line were constrained in the horizontal direction. The displacements of the rigid surface were controlled through a reference node, and the reactant force of the reference node was calculated. The numerical modeling of the shape configuration processes followed the same four steps used in the experiment (described previously). Figure 12 shows the comparison between the numerical simulation and the experiments. Figure 13 shows the breakdown of each thermomechanical cycle. We observed that the FE simulations of the shape-recovery processes with the Ogden model agreed very well with the experimental measurements.

CONCLUSIONS

An epoxy-based SMP was fabricated as a candidate material for reconfigurable structures and devices. The stress–stain behaviors of the SMP were characterized through compressive tests at various temperatures. Overall, the SMP exhibited nonlinear, finite deformation in all regions. To capture the complex stress–strain responses across various temperature regimes, strain-energy-based modeling was used. Among all of the models, the stretch-based Ogden model provided the best fit to the stress–strain responses. The shape-recovery ability of the SMP was also examined according to the standard programing cycle. The results show that the SMP could fully recover its original shape under unconstrained conditions. The shape-recovery processes could be simulated well by the Ogden model.

ACKNOWLEDGMENTS

This work was supported by a grant from the National Science Foundation (contract grant number CMS-1130381).

APPENDIX

Summary of the Experimental Stress–Strain Data of the SMP

Table A.I summarizes the nominal stress–strain data of the SMP at various temperatures. The data were entered as nominal strain–nominal stress under Uniaxial Test Data in the unit-cell FE model.

Table A.I. Experimental Stress–Strain Data for the SMP Used in the FE Model

Strain	Stress (MPa)				
	30°C	35°C	45°C	50°C	55°C
0.000	0.156	0.690	0.006	0.546	0.038
0.020	10.130	7.066	2.486	0.829	0.175
0.040	16.920	12.480	3.682	1.078	0.359
0.060	20.580	15.630	4.397	1.327	0.590
0.080	22.760	17.650	4.875	1.545	0.804
0.100	24.280	19.000	5.312	1.794	1.035
0.120	25.250	20.110	5.621	2.046	1.356
0.140	26.120	21.030	6.054	2.387	1.617
0.160	26.890	21.800	6.457	2.670	1.891
0.180	27.610	22.350	6.830	2.998	2.152
0.200	28.210	22.910	7.233	3.373	2.550
0.220	28.900	23.460	7.637	3.779	2.854
0.240	29.510	24.000	8.135	4.198	3.192
0.260	30.160	24.590	8.599	4.652	3.650
0.280	30.870	25.190	9.172	5.184	4.142
0.300	31.520	25.960	9.731	5.713	4.617
0.320		26.800	10.370	6.306	5.152
0.340		27.870	11.170	7.009	5.764
0.360		29.350	11.980	7.776	6.132
0.380		31.040	12.910	8.601	
0.400		33.360	14.010	9.618	
0.420			15.250	10.820	
0.440			16.630	12.270	
0.460			18.020	14.000	
0.480				16.160	

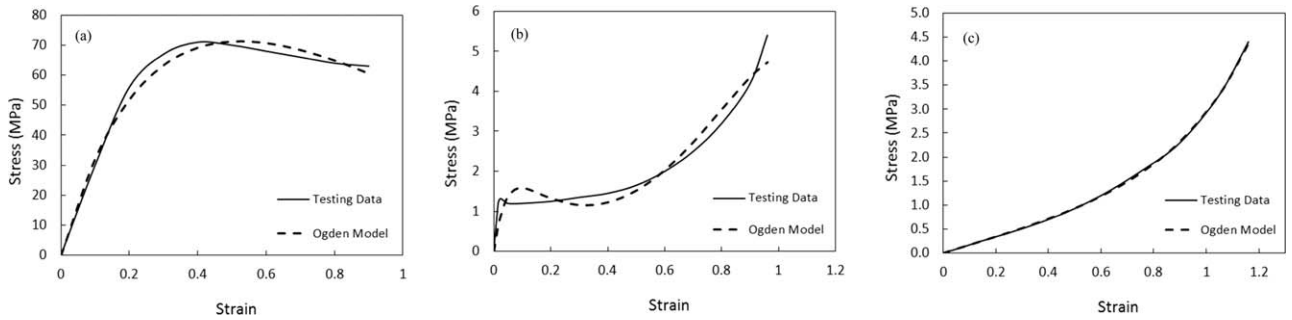

Figure A.1. Predictions of the stress–strain responses of an epoxy-based SMP with the Ogden model: (a) 25, (b) 90, and (c) 130°C.

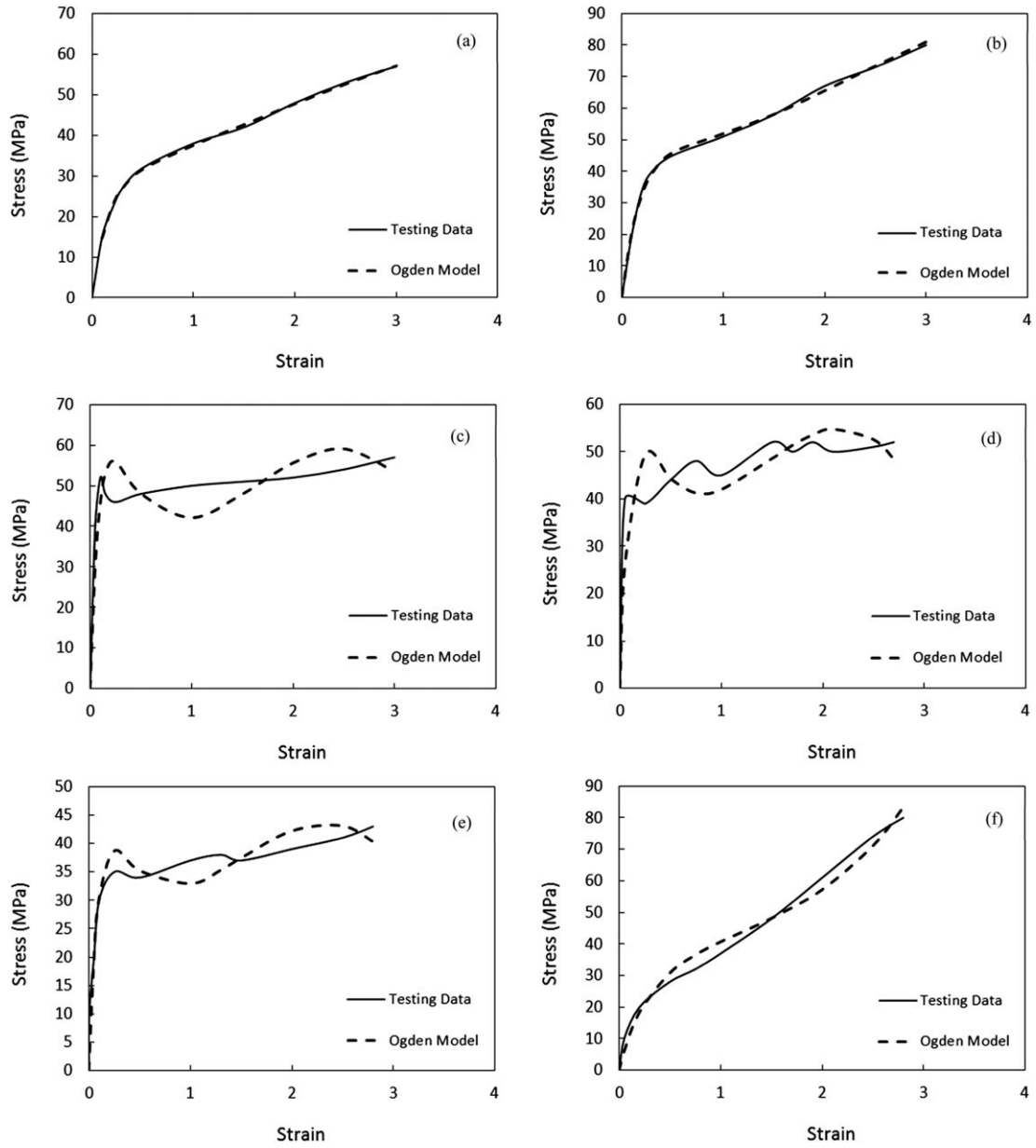

Figure A.2. Predictions of the stress–strain responses of an aramid-based SMP with the Ogden model: (a) P2, (b) P6, (c) P8, (d) P11, (e) P16, and (f) P18.

Table A.II. Details of the Compositions, Molar Mass Averages, and Transition Temperatures of a Series of Aramid-Based SMPs

Polymer	Composition	M_n (g/mol	T_g (°C)
P2	PCL4200:T1 (2:1)	110,000	−52
P6	PCL4200:T3 (2:1)	100,000	−58
P8	PCL4200:T4 (5:1)	170,000	−59
P11	PCL8200:T1 (1:1)	110,000	−57
P16	PCL8200:T3 (1:4)	90,000	−60
P18	PCL8200:T4 (1:5)	70,000	−48

M_n, number-average molecular weight; PCL, polycaprolactone; T, telechelics.

VALIDATION OF THE OGDEN MODEL WITH ADDITIONAL SMP MATERIAL SYSTEMS

The Ogden model was further tested with two additional SMP material systems: an epoxy-based SMP[23] and an aramid-based SMP.[24]

The epoxy-based SMP had a T_g of 105°C. The stress–strain responses of the SMP were comprehensively characterized at various regions (glassy, transitional, and rubbery regions) by tensile testing.[23] The comparisons of the Ogden model and experimental measurements for the epoxy-based SMP are shown in Figure A.1.

The aramid based SMP was synthesized by the reaction of an aminobenzoyl-terminated polycaprolactone with terephthaloyl chloride. A series of SMPs were subsequently made by the modification of the polycaprolactone composition, as summarized in Table A.II. The stress–strain responses of the SMPs were characterized at room temperature by tensile testing.[24] The comparisons of the Ogden model and experimental measurements for the aramid-based SMP are shown in Figure A.2.

Overall, the Ogden model provided good predictions of the stress–strain responses of these materials.

REFERENCES

1. Keihl, M. M; Bortolin, R. S; Sanders, B; Joshi, S; Tidwell, Z. In SPIE Conference: Smart Structures and Materials—Industrial and Commercial Applications of Smart Structures Technologies: San Diego, CA, **2005**; Vol. *5762*, p 143.
2. Flanagan, J. S; Strutzenberg, R. C; Myers, R. B; Rodrian, J. E. In 48th AIAA/ASME/ASCE/AHS/ASC Structures, Structural Dynamics, and Materials Conference, Honolulu, Hawaii; AIAA 2007-1707; American Institute of Aeronautics and Astronautics: Reston, VA, **2007**; pp 1, 23.
3. Love, M. H; Zink, P. S; Stroud, R. L; Bye, D. R; Rizk, S; White, D. In 48thAIAA/ASME/ASCE/AHS/ASC Structures, Structural Dynamics, and Materials Conference, Honolulu, Hawaii; AIAA 2007-1729; American Institute of Aeronautics and Astronautics: Reston, VA, **2007**; p 1–12.
4. Bye, D. R.; McClure, R. D. In 48th AIAA/ASME/ASCE/AHS/ASC Structures, Structural Dynamics, and Materials Conference, Honolulu, Hawaii; AIAA 2007-1728; American Institute of Aeronautics and Astronautics: Reston, VA, **2007**; pp 1, 23.
5. Toensmeir, P. A. *Aviation Week Space Technol.* **2005**, *5*, 72.
6. Leng, J.; Lan, X.; Liu, Y.; Du, S. *Prog. Mater. Sci.* **2011**, *56*, 1077.
7. Tobushi, H.; Hashimoto, T.; Hayashi, S.; Yamada, E. *J. Intell. Mater. Syst. Struct.* **1997**, *8*, 711.
8. Tobushi, H.; Ito, N.; Takata, K.; Hayashi, S. *Shape Memory Mater.* **2000**, *327-3*, 343.
9. Bhattacharyya, A.; Tobushi, H. *Polym. Eng. Sci.* **2000**, *40*, 2498.
10. Hong, S. J; Yu, W. R; Youk, J. H. *AIP Conf. Proc.* **2007**, *907*, 853.
11. Srinivasa, A. R.; Gosh, P. *AIP Conf. Proc.* **2008**, *1029*, 58.
12. Liu, Y.; Gall, K.; Dunn, M. L.; Greenberg, A. R.; Diani, J. *Int. J. Plast.* **2006**, *22*, 279.
13. Chen, Y. C.; Lagoudas, D. C. *J. Mech. Phys. Solids.* **2008**, *56*, 1752.
14. Chen, Y. C.; Lagoudas, D. C. *J. Mech. Phys. Solids.* **2008**, *56*, 1766.
15. Qi, H. J.; Nguyen, T. D.; Castroa, F.; Yakacki, C. M.; Shandasa, R. *J. Mech. Phys. Solids* **2008**, *56*, 1730.
16. Rivlin, R. S. *Philos. Trans. R. Soc. A* **1948**, *241*, 379.
17. Yeoh, O. H. *Rubber Chem. Technol.* **1993**, *66*, 754.
18. Ogden, R. W. *Proc R. Soc. Lond. A* ***1972***, 326, *565.*
19. Steinmann, P.; Hossain, M.; Possart, G. *Arch. Appl. Mech.* **2012**, *82*, 1183.
20. Treloar, L. R. G. The Physics of Rubber Elasticity; Clarendon: Oxford, **1975**.
21. Arruda, E. M.; Boyce, M. C. *J. Mech. Phys. Solids* **1993**, *41*, 389.
22. ABAQUS Users' Manual; Dassault Systèmes: Pawtucket, RI, **2013**.
23. McClung, A. J. W.; Tandon, G. P.; Baur, J. W. *Mech. Time-Depend. Mater.* **2012**, *16*, 205.
24. Schuh, C.; Schuh, K.; Lechmann, M. C.; Garnier, L.; Kraft, A. *Polymers* **2010**, *2*, 71.
25. Xie, T.; Rousseau, I. A. *Polymer* **2009**, *50*, 1852.